https://doi.org/10.52131/jmps.2020.0102.0010

Journal of Materials and Physical Sciences

Volume 1, Number 2, 2020, Pages 98 - 108

Journal Homepage:
https://journals.internationalrasd.org/index.php/jmps

Synthesis and Characterization of Praseodymium Doped Nickel Zinc Ferrites using Microemulsion Method

H. M. Noor ul Huda Khan Asghar[1], Muhammad Kamran Nawaz[1], Rafaqat Hussain[1], Zaheer Abbas Gilani[1*]

[1] Department of Physics, Balochistan University of Information Technology, Engineering & Management Sciences, Quetta 87300, Pakistan

ARTICLE INFO

Article History:
Received: October 03, 2020
Revised: November 27, 2020
Accepted: December 29, 2020
Available Online: December 31, 2020

Keywords:
Praseodymium
Nickel–Zinc Ferrite
Spinal Ferrites
Microemulsion
XRD
FTIR
Dielectric Properties

ABSTRACT

Spinel ferrites nanoparticles are plays important role in our daily life. Praseodymium doped Nickel Zinc Ferrite Nanoparticles having general formula $Ni_{0.3}Zn_{0.7}Pr_xFe_{2-x}O_4$ (x=0.00, 0.025, 0.050, 0.075 and 0.1) were synthesized by microemulsion method. X-Ray diffraction (XRD) was used to find different parameters of crystalline size. The development of the FCC spinel structure was observed by XRD data. The most intense peak of the XRD was identified at 2θ=35º.From Debye sherrer's formula, calculated the crystalline size 15nm to 29nm ranges. The lattice constant calculations are decreased with the doping of Praseodymium (Pr^{3+}) contents. The x-ray density increases as the concentration of Praseodymium (Pr^{3+}) doping increases, Because Praseodymium (Pr^{3+}) ion has a greater molar weight than Fe^{3+} ion. The Absorption band spectra are analyzed by using Fourier Transform Infrared spectroscopy (FTIR). The absorption bands υ1 is known as octahedral stretching bands were found to be in the range of 414 cm^{-1} and υ_2 is the tetrahedral stretching band were found to be in the range of 530cm^{-1}. Dielectric properties of Praseodymium doped Nickel-Zinc Ferrite were measured with impedance Analyzer in the frequency of 1 MHz to 3 GHz range. When Pr^{3+} content concentration increases, the dielectric characteristics, such as dielectric constant, dielectric loss, and tangent loss were also decreased. These measured dielectric characteristics showed that these nanomaterials may be used in higher frequencies devices.

*Corresponding Author's Email: zagilani2002@yahoo.com

1. Introduction

Developments in nanotechnology have revealed a successful applications for several materials that will be used in advanced technologies (Ahmed, Bishay, & Radwan, 2002). Ferrites have attracted the attention of scientists and researchers due to their numerous applications in transformer cores, magnetic memories, high-frequency circuits, and electronic circuits. Semiconductors and magnetic materials have unique features, and they are used in a variety of electrical device (Muhammad Azhar Khan, Islam, Ishaque, & Rahman, 2012). The chemical formula for spinel ferrites is AB_2O_4 (Lodhi et al., 2014). Many methods have been developed to improve the fundamental features of nano-ferrites by including other metal ions and using different production techniques. Rare earth ions are an excellent substitute for increasing spinel ferrites characteristics (M Azhar Khan, Islam, Ishaque, & Rahman, 2011). Soft Ni-Zn ferrites are inexpensive materials with intriguing electrical and magnetic properties. Microwave devices such as isolators, transformers, and

circulators have all used these ferrites (Al-Hilli, Li, & Kassim, 2009). Chemical composition, annealing process, and kind of doped metal ions all influence the inherent properties of ferrites, such as permittivity, dielectric losses, and conductivity (Al-Hilli, Li, & Kassim, 2012; Jing, Liangchao, & Feng, 2007). Several synthetic processes, including as coprecipitation, sol–gel, microemulsion, ceramic, and hydrothermal methods are used to produce high-quality doped praseodymium spinel ferrites (Sun & Sun, 2007). The rare earth doped Nickel-Zinc ferrites are prominent, Due to their significance in microwave devices. The incorporation of metal ions with larger ionic radii into the spinel structure results in structural distortion as well as changes in electrical and dielectric features. In compared to other simple ferrites, the different forms of substitution in Nickel-Zinc ferrites indicate a reasonably good relaxation and conduction mechanism (Iqbal, Islam, Ali, Sadiq, & Ali, 2014). According to researches, different rare earth ions doping modifies the behaviour of spinel ferrites (Al-Hilli et al., 2012). Furthermore, doping rare earth elements in these nanomaterials can improve electrical properties and optical properties. A lot of study has gone into changing the characteristics of ferrites by doping rare earth cations in these ferrites (Sun & Sun, 2007). The influence of Pr^{3+} concentration on structural, spectral, and dielectric properties has been presented in this work. $Ni_{0.3}Zn_{0.7}Pr_xFe_{2-x}O_4$ (x= 0.0, 0.025, 0.05, 0.075 and 0.1) spinel ferrites was prepared via a micro-emulsion technique. The purpose of this research is to improve the structural and dielectric properties of these nanocrystalline ferrites so that they can be used in the manufacture of microwave devices (Junaid et al., 2016).

2. Experimental Procedure

Praseodymium doped Nickel−Zinc ferrites with general formula $Ni_{0.3}Zn_{0.7}Pr_xFe_{2-x}O_4$ (x= 0.0, 0.025, 0.05, 0.075 and 0.1) was synthesized by using Microemulsion Method. This method wasuseful because it reduces cation nucleation compared to other methods such as sol-gel and co-precipitation. The chemicals were used for preparation of solution are as follows: Nickel nitrate-6 hydrate ($Ni(NO_3)_2.6H_2O$)(M.W=290.81)(99%), Zinc Nitrate Hexahydrate ($N_2O_6Zn.6H_2O$)(M.W=297.46)(98%), Praseodymium Nitrate Hexahydrate ($N_3O_3Pr.H_2O$) (M.W=435.01)(99.9%), Iron(III) Nitrate9 hydrate ($FeN_3O_9.9H_2O$) (M.W=404) (98%), Cetyltrimethylammonium bromide ($C_{19}H_{42}BrN$) (M.W=346.45) (99%) were weighted using precise digital balance. The Praseodymium, Nickel, Zinc and iron sample solutions were prepared in distilled water, then combined to produce the mixed solution. The magnetic stirrer was used to stir the solution at 50°C. CTAB solution was added to the mixture of the solution. Aqueous ammonia solution was added to maintain the PH value up to 10. The mixture of all samples were stirred continuously for 5 hours. After stirring, all of the $Ni_{0.3}Zn_{0.7}Pr_xFe_{2-x}O_4$ solutions were placed in the cupboards overnight. During this time, the precipitation was settled down. To reduce the value of PH, all samples were washed with deionized distilled water. The washing was carried out until the PH value reached a neutral level of 7. To remove the water, the samples of various compositions were dried in a thermostat oven at about 80 °C. Methanol was used to clean and wash the mortar and pestle before grinding. The samples were grinded in a mortar and pestle after drying. After each grinding, the mortar and pestle were washed and dried to avoid contamination. All samples were placed in muffle furnace for annealing at 700˚C for 3 hours. The samples was pelletized with a 4.5 ton pressure by using Hydraulic press. The prepared ferrites samples were characterized by using different characterization techniques, The XRD was done using a PANalytical XPert Pro to examine the crystal structure and determine numerous crystalline structure parameters. The Tetrahedral and octahedral stretching bands were investigated using FTIR. The dielectric characteristics of synthesized ferrite material were investigated using an impedance analyzer. Different dielectric properties, including as the dielectric constant, dielectric loss, tangent loss, AC conductivity, real and imaginary parts of impedance, and modulus, were calculated in the frequency range of 1MHz to 3GHz, and their variations were investigated as Pr^{3+} content increased.

3. Results and Discussion

3.1. XRD Analysis

Praseodymium doped Nickel Zinc Ferrite Nanoparticles having general formula $Ni_{0.3}Zn_{0.7}Pr_xFe_{2-x}O_4$ (X=0.00, 0.025, 0.05, 0.075and 0.1) was effectively prepared by microemulsion technique. The samples were annealed at temperature of 700℃ for 5hours.

XRD was used to analysis crystal structure and the formation of crystalline phase powder, which is a very useful technique for calculating crystalline parameters such as crystalline size, lattice constant, bulk density, x-Ray density and dislocation density etc. The XRD pattern shows very sharp peaks, indicating the formation of the crystalline phase of Nickel-Zinc ferrite. The most intense peak on the XRD was identified at 2θ=35º, which is considered to be the most intense peak for cubic spinel structure. The peaks that correspond to the XRD trend are evaluated and assigned the numbers (220), (311), (400), (422), (511), (440), and (531) correspondingly. The FCC spinel structure is defined by these peaks.JCPDS card number 22-1086 confirms these peaks. Two impurity peaks can be seen, one at 2θ =33.27º and the other at 2θ =49.54º. These impurity peaks could be caused by Pr^{3+} insolubility in the octahedral site (Sheikh et al., 2019).

The crystalline size of the prepared ferrites can be determined by using the Debye sherrer's formula given as:

$$D_m = \frac{k\lambda}{\beta \cos\theta} \quad (1)$$

In the above equation 'k' is equal to 0.9 (constant), λ is wavelength of x-ray in Å. β is FWHM for intense peak of XRD, θ is the Bragg diffraction angle. The crystalline size was determined to be in the 15nm to 29nm range. With the substitution of Pr^{3+}, the crystalline size varied in an inhomogeneous form. This inhomogeneous behavior of crystalline size is due to the formation of a secondary phase (Warsi et al., 2017).

The Nelson Relay Function determines the lattice constant as a function of Pr^{3+} concentration, which is given as:

$$a = d\,(h^2 + k^2 + l^2)^{1/2} \quad (2)$$

Where 'hkl' is the index of the XRD reflection peak and 'd' is the inter planer spacing. The Average lattice constant in the range of 8.360Å−8.380Å. First Lattice constant decreases with increase of Pr^{3+} substitution ion contents and then increases, finally at the end Lattice constant decreases (Aslam et al., 2019). The X-ray density of the prepared nanoferrites was calculated by using the following formula as:

$$\rho x = 8M/NAa^3 \quad (3)$$

Where 'M' denotes molecular weight, 'NA' denotes Avogadro's number, and a^3 denotes the lattice constant. The X-ray density varies from 5.39 to 5.62 g/cm^3 depends upon the concentration. It is also observed that X-Ray Density and concentration are approximately linear. As Pr^{3+} concentration is increased, X-Ray density also increased (Gao, Wang, Pei, & Zhang, 2018). The Bulk density was calculated by using the formula give as:

$$\rho_m = m/v \quad (4)$$

Where 'm' is mass of prepared pellets and 'v' is volume of the prepared pellets. Bulk Density varies between 3.07 to 3.58 g/cm^3. Bulk Density shows an in-homogeneous variance with concentration. The bulk density first increases then decreases and then again increases and the end it again decreases due to the concentration of pr^{3+} doping. The Lattice strain (ε) of the ferrites was determined by formula given as:

$$\varepsilon = \beta/4 * \tan\theta \ (10^{-3}) \quad (5)$$

The Lattice strain was calculated to be in the range of 3.92 $\times 10^{-3}$ to 7.19 $\times 10^{-3}$. The Lattice strain was found to be increases in-homogeneously with respect to concentration of Pr^{3+} substituent. The value of Lattice strain is maximum at x= 0.075 and then decreases. The Micro-strain of prepared Ferrites was calculated by using the following formula:

$$\text{Micro-strain} = \beta \times \cos\theta/4 \ (10^{-3}) \quad (6)$$

Where β is FWHM of most intense peak XRD. The Micro Strain Values was calculated to be in the range of 1.16 $\times 10^{-3}$ to 2.18 $\times 10^{-3}$. The Micro-stain was found to be increases

with respect to concentration of Pr^{3+} substituent. The Micro-Strain value is maximum at concentration of Pr^{3+} substituent is at x= 0.075. The Dislocation density of prepared samples was determined by following formula:

$$\delta = 1/D^2\ (10^{15}) \quad (7)$$

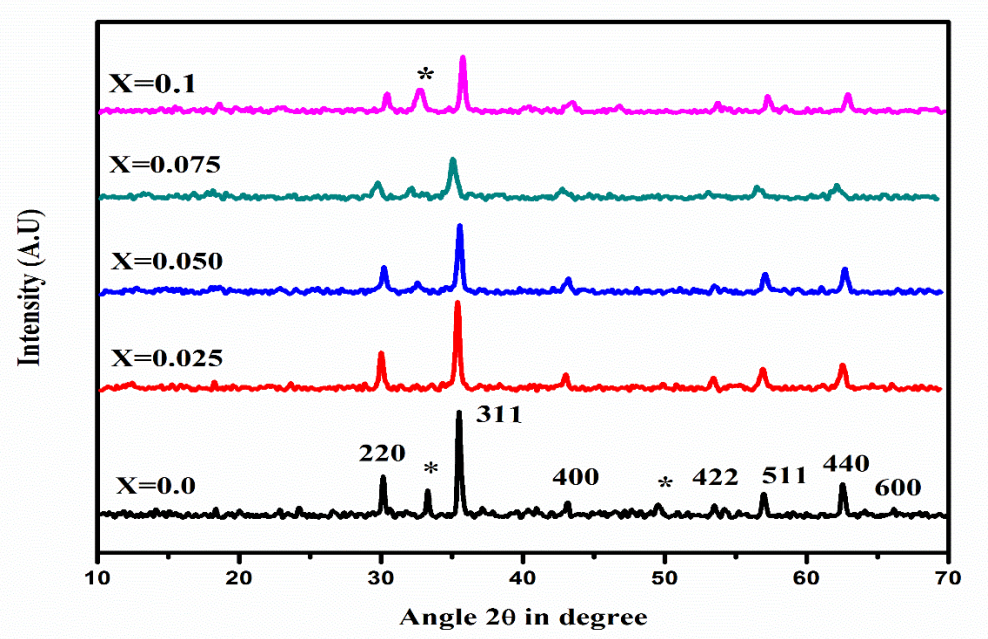

Figure 1: XRD analysis of $Ni_{0.3}Zn_{0.7}Pr_xFe_{2-x}O_4$ (x=0.00, 0.025, 0.050, 0.075 and 0.1)

Where 'D' is the crystalline size, The Dislocation Density was measured to be in the range of 4.20×10^{15} to 7.27×10^{15}. The Dislocation density was found to be increases with respect to concentration of Pr^{3+} substituent. The Dislocation density value is maximum at concentration of Pr^{3+} substituent is at x= 0.075. The Stacking Fault of the prepared nanoparticles is calculated by the formula:

$$\text{Stacking Fault} = 2\,\pi^2/45\sqrt{3}(\tan\theta) \quad (8)$$

The stacking fault was observed to be decreases and then increases to a certain value, and again finally decreases. This inhomogeneous behaviour of the Stacking Fault is due to annealing temperature (Brightlin & Balamurugan, 2016).

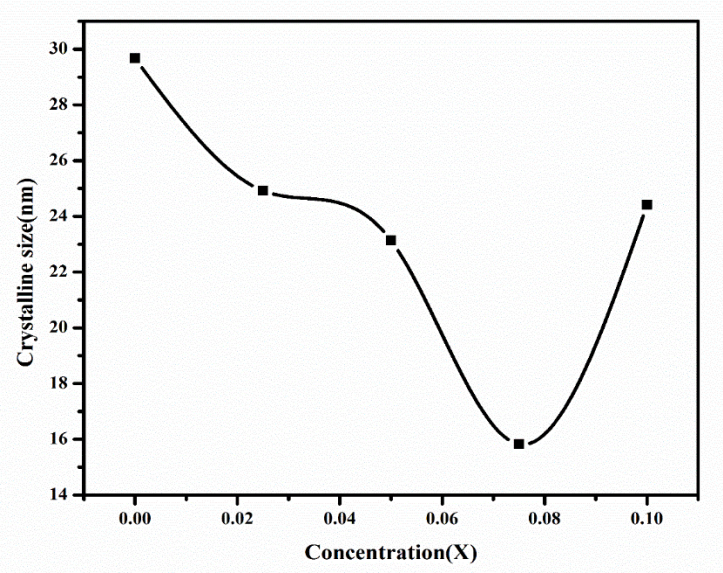

Figure 2: Concentration Vs Crystalline size of $Ni_{0.3}Zn_{0.7}Pr_xFe_{2-x}O_4$ (x=0.00, 0.025, 0.050, 0.075 and 0.1)

Table 1
Different structural parameters of XRD for composition of $Ni_{0.3}Zn_{0.7}Pr_xFe_{2-x}O_4$ (x=0.00, 0.025, 0.050, 0.075 and 0.1)

Parameter	x = 0	x = 0.025	x = 0.05	x = 0.075	x = 0.1
Crystalline size (nm)	29.672	24.920	23.133	15.825	24.414
Lattice constant a(Å)	8.379	8.371	8.367	8.374	8.360
Cell Volume (a^3)	588.295	586.507	585.843	587.306	584.358
X-Ray Density (g/cm^3)	5.398	5.463	5.517	5.552	5.628
Bulk Density (g/cm^3)	3.0738	3.4262	3.2135	3.5834	3.4429
Lattice Strain$\times10^{-3}$	3.92261	4.55211	4.9105	7.1933	4.6544
Micro Strain$\times10^{-3}$ ($lines^{-2}/m^{-4}$)	1.1678	1.3904	1.49786	2.18945	1.4192
Dislocation Density$\times10^{15}$ ($lines/m^2$)	4.2079	5.0194	4.5202	7.2736	6.0952
Stacking Fault	0.4473	0.4467	0.4470	0.4475	0.4471

3.2. FTIR Spectroscopy

Fourier Transform Infrared Spectroscopy (FTIR) is a technique used to investigate spinel crystal structure of the prepared sample of composition $Ni_{0.3}Zn_{0.7}Pr_xFe_{2-x}O_4$ (x=0.00, 0.025, 0.050, 0.075 and 0.1). The FTIR spectra shows two frequency bands, one of which is higher frequency band υ_2 at around 530 cm^{-1} and the second is lower frequency band υ_1, at around 400 cm^{-1}. These samples have cubic spinel structure since the two main absorption bands υ_1 is known as octahedral stretching bands are found to be in the range of 414 cm^{-1} and υ_2 is the tetrahedral stretching band are found to be in the range of 530cm^{-1}. The tetrahedral and octahedral frequency bands are investigated in this analysis. Because of the tetrahedral site of intrinsic stretching vibrations, the absorption peaks are called high frequency bands υ_1. Octahedral stretching bands are covered by low frequency band υ_2 (Batoo et al., 2017). The characteristics feature of spinel ferrite structure are shown in these bands.it is observed that low frequency band υ_1 value remains static. The lattice constant variations were responsible for the slight shift of high frequency band υ_2 and low frequency band υ_2 towards higher frequency bands with an increase in Pr^{3+} constituent. The Fe^{3+}-O^{2-} stretching vibrations were influenced by the change in lattice constant, resulting in a shift in band position (Gilani et al., 2015). The tetrahedral and octahedral sites for force constants K_0 and K_t have been calculated using the following relations:

$$Ko = 0.942128M\ (\upsilon_2)^2/\ (M+32) \quad (9)$$

$$K_t = \sqrt{2}Ko\ \upsilon_1/\ \upsilon_2 \quad (10)$$

Where 'M' is molecular weight of prepared samples, υ_1 and υ_2 are the frequency bands. The tetrahedral and octahedral Radii was calculated by using the following formulas:

$$R_t = a\sqrt{3}\ (u-0.25) - Ro \quad (11)$$

$$R_o = a\ (5/8-u) - Ro \quad (12)$$

Where 'a' is lattice constant and 'u' is oxygen positional parameter, the value of oxygen positional parameter is 0.375.

Table 2
Different parameters in FTIR studies

Parameters	x = 0.0	x = 0.025	x = 0.05	x = 0.075	x = 0.1
Molecular weight (gm/mol)	239.06402	241.19059	243.31715	245.44372	247.57029
υ_1 (cm^{-1})	540	537	540	537	540
υ_2 (cm^{-1})	414	414	414	414	414
K_o($dyne/cm^{-1}$)*10^5	1.424141	1.425625	1.427086	1.428524	1.429941
K_t($dyne/cm^{-1}$)*10^5	2.627008	2.615135	2.63244	2.620454	2.637707
R_0	0.080733	0.079958	0.079649	0.080419	0.080488
R_t	0.052232	0.051561	0.051293	0.05196	0.05202

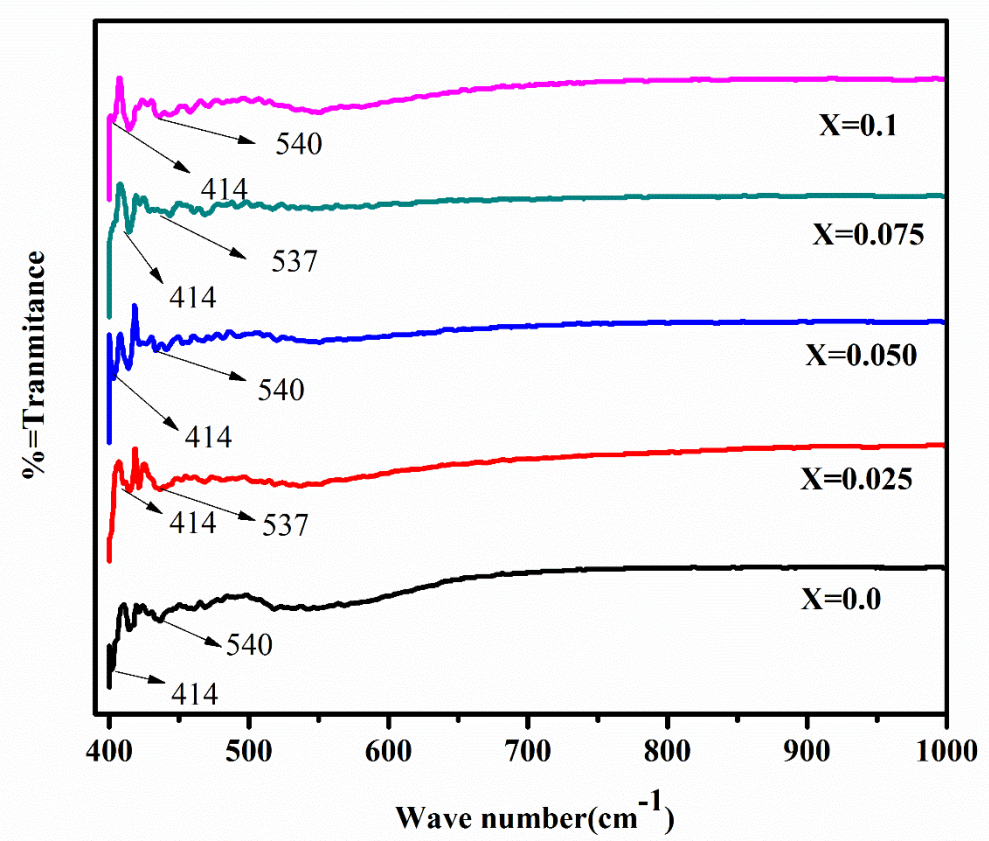

Figure 3: FTIR spectra of $Ni_{0.3}Zn_{0.7}Pr_xFe_{2-x}O_4$ (x=0.00, 0.025, 0.050, 0.075 and 0.1)

3.3. Dielectric Properties

The dielectric properties of synthesized Praseodymium doped Ni-Zn Ferrite Nanoparticles having general formula $Ni_{0.3}Zn_{0.7}Pr_xFe_{2-x}O_4$ (x=0.00, 0.025, 0.050, 0.075, and 0.1) were measured using an impedance analyzer. These characteristics are critical in determining the prepared ferrite is suitable for use in ultra-high-frequency devices. The synthesis technique, material composition, and cation orientation all affect these properties. The dielectric characteristics of synthesized ferrite nanoparticles were determined from 1 MHz to 3 GHz (Parveen et al., 2019).

3.3.1. Dielectric Constant and Dielectric Loss

The Figure 4(a) and Figure 4(b) shows the dielectric constant (ε') and dielectric loss (ε'') decreases with increasing of frequency. In electron conduction, grain boundaries had a significant impact as compared to grains at low frequencies. The free and localized charge carriers were identified based on the observed dielectric constant and losses. The normal dielectric dispersion was observed that the dielectric constant dropped as frequency raised. At low frequencies, dispersion can contribute to the polarization phenomenon. The reduction in dielectric constant was attributed to both Maxwell Wagoner's model and Koop's theory. It was thought that dielectric material was made up of well-conducting regions called grains that were separated by resistive regions called grain boundaries. Since charge carriers are displaced locally, polarization occurs between Fe^{2+} and Fe^{3+} at grain boundaries which are in octahedral sites. The hopping mechanism causes electrons to accumulate at grain boundaries due to high resistance, resulting in space charge polarization. Dielectric dipoles that followed the variance in applied field provided a high dielectric constant at low frequencies (Junaid et al., 2016).

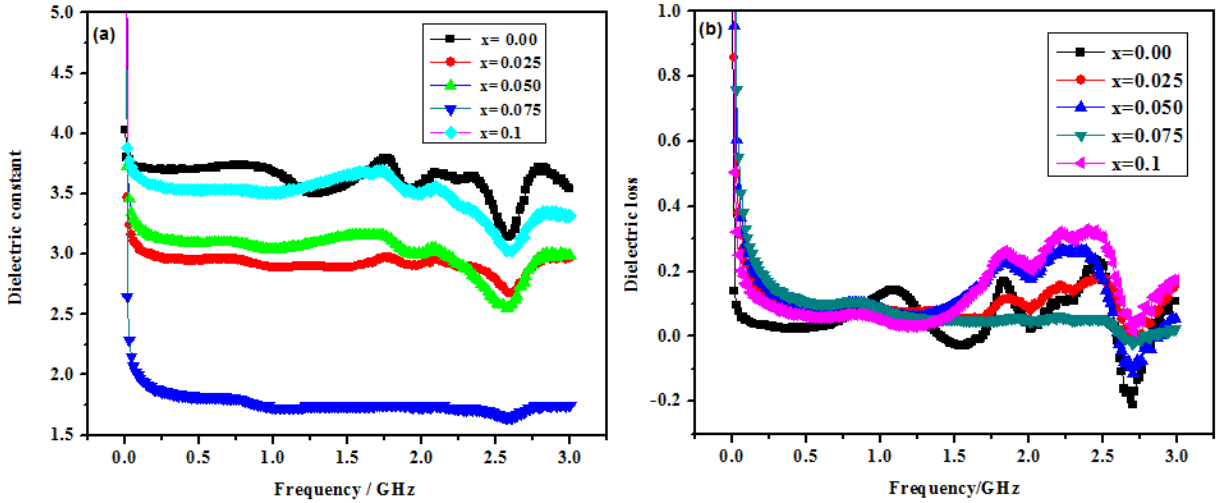

Figure 4: (a) Dielectric constant Vs Frequency (b) Dielectric loss Vs Frequency

Table 3
Different parameters of Dielectric properties for $Ni_{0.3}Zn_{0.7}Pr_xFe_{2-x}O_4$ (x=0.00, 0.025, 0.050, 0.075 and 0.1)

Parameters	Frequency	x = 0.00	x = 0.025	x = 0.05	x = 0.075	x = 0.1
Dielectric constant	1MHZ	4.027146	8.191817	8.638792	8.521431	6.476407
	1GHZ	3.684943	2.891025	3.039607	1.732787	3.506363
	3GHZ	3.538591	2.970498	2.993035	1.748285	3.317121
Dielectric loss	1MHZ	1.047309	6.292897	7.818412	9.375467	3.352912
	1GHZ	0.1281894	0.08786879	0.08285637	0.08466826	0.04852595
	3GHZ	0.1014174	0.1603908	0.05450426	0.0221134	0.1812719
Tangent loss	1MHZ	0.2600623	0.768193	0.9050353	1.100222	0.5177118
	1GHZ	0.03478736	0.03039364	0.02725891	0.04886246	0.0138394
	3GHZ	0.02866039	0.05399459	0.01821036	0.01264863	0.05464737
AC Conductivity	1MHZ	$4.37885E^{-05}$	0.00033173	0.00040391	0.000498323	0.000221814
	1GHZ	0.01166646	0.00647035	0.00611162	0.007627428	0.003629156
	3GHZ	0.01846953	0.03341900	0.0102711	0.00463901	0.03693199

3.3.2.Tan Loss and AC Conductivity

Tan loss variance is examined that $Ni_{0.3}Zn_{0.7}Pr_xFe_{2-x}O_4$ (x=0.00, 0.025, 0.050, 0.075, and 0.1) nano ferrite is inversely proportional to the applied frequency. Tangent loss reduced as frequency increased. The conduction phenomena was connected to electron hopping between Fe^{2+} and Fe^{3+} ions. Since the applied and hopping frequencies were matched, the maximum loss occurred at a high frequency (Junaid et al., 2016). The variance of Tangent loss with frequency shows in the below Figure 5(a). The most important properties of dielectric materials is AC conductivity. At room temperature, the AC conductivity of $Ni_{0.3}Zn_{0.7}PrxFe_{2-x}O_4$(x=0.00, 0.025, 0.05, 0.075, and 0.1) synthesized nanoferrites was determined in frequency range is between 1 MHz and 3 GHz. The formula for calculating AC conductivity is as follows:

$$\sigma_{ac} = (t/A)\, z'/(z'^2+z''^2) \qquad (13)$$

From the above formula 't' denotes pellet thickness, 'A' denotes area, z' denotes the real impedance part, and z'' denotes the imaginary impedance part. The Figure 5(b) shows that, at lower frequency the AC conductivity of most samples have a growing pattern, but in the higher frequency region dispersive behavior of samples. According to the Maxwell Wagner theory, ferrites materials are composed of conducting grains separated by a resistive layer of grain boundaries. Reduced porosity may also be causing the increase in conductivity behavior. Conductivity has a grain boundary effect at low frequencies, while conducting effects of grains have been found at high frequencies, resulting in dispersion. Because of the impacts of grains and the hopping phenomena in Fe^{2+} and Fe^{3+} at octahedral sites, conductivity improves at high frequencies. As the applied field increases, the charge

carrier hopping frequency increases, resulting in an increase in ac conductivity (Junaid et al., 2016; Parveen et al., 2019).

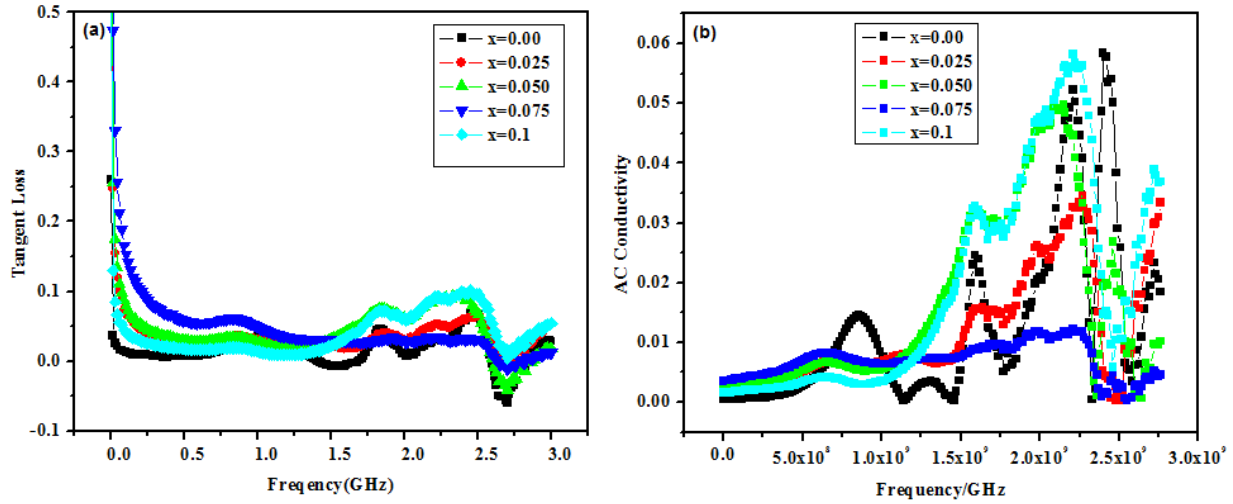

Figure 5: (a) Tangent loss Vs Frequency (b) AC Conductivity Vs Frequency

3.4.4.Real and Imaginary Impedance

Impedance analysis is a useful method for determining the relationship between dielectric properties and microstructural composition of synthesized materials. For each of the ferrite $Ni_{0.3}Zn_{0.7}Pr_xFe_{2-x}O_4$(x=0.00, 0.025, 0.05, 0.075, and 0.1), the real and imaginary impedance parts was calculated, the real part of impedance as a function of Log F is shown in Figure 6 (a) and the imaginary part of impedance as a function of log F is shown in Figure 6 (b).

The following formulas are used to calculate the impedance of the real and imaginary parts.

$$Z' = R = |Z|Cos\theta_z \quad (14)$$

$$Z' = X = |Z|Sin\theta_z \quad (15)$$

From the figures 6. (a) And (b), as the frequency rises, the real and imaginary parts of impedance decreases according to impedance analysis. As frequency increases, the impedance curves of all samples converged, and at higher frequencies, impedance shows constant behavior, which is attributed to the discharge of space charges. The concentration differential as well as the inhomogeneity of the applied field lead these charges to collect on grain boundaries, resulting in space charges. The real and imaginary impedance parts decrease as the field frequency increases, indicating that conductivity improves.

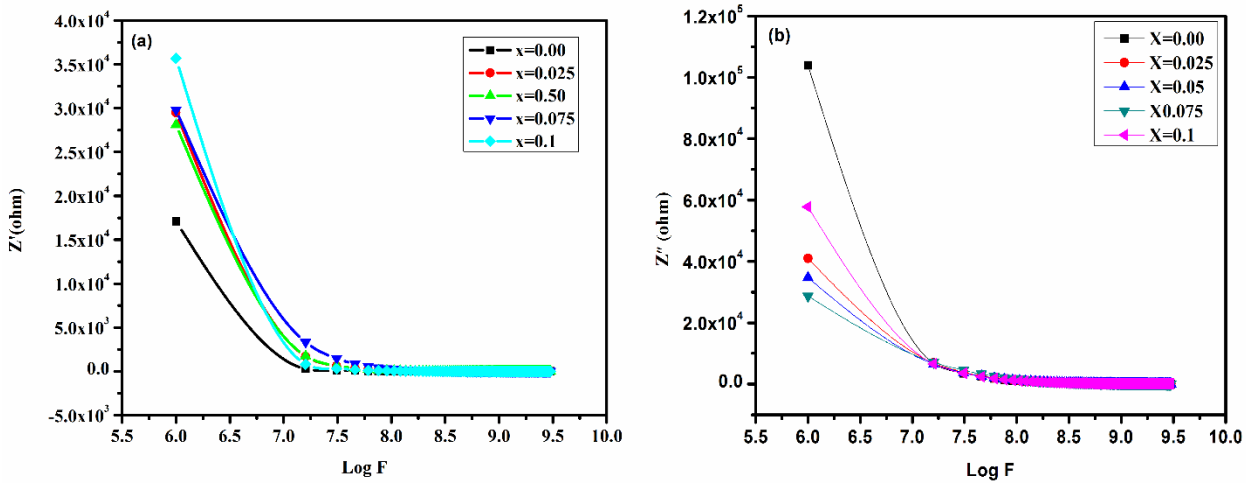

Figure 6: (a) Real part of Impedance Vs Log F and (b) imaginary part of Impedance Vs Log F

Table 4
Impedance and Modulus for $Ni_{0.3}Zn_{0.7}Pr_xFe_{2-x}O_4$ (x=0.00, 0.025, 0.050, 0.075 and 0.1)

Parameters	Frequency	x =0.00	x = 0.025	x = 0.05	x = 0.075	x = 0.1
	1MHZ	1.71E+04	2.95E+04	2.81E+04	2.98E+04	3.57E+04
Z' (ohm)	1GHZ	4.96E+00	3.87E+00	3.41E+00	8.96E+00	1.67E+00
	3GHZ	9.54E-01	2.15E+00	6.57E-01	6.05E-01	2.08E+00
	1MHZ	1.04E+05	4.10E+04	3.47E+04	2.87E+04	5.78E+04
Z'' (ohm)	1GHZ	1.10E+02	1.31E+02	1.26E+02	1.83E+02	1.15E+02
	3GHZ	3.85E+01	4.29E+01	4.28E+01	6.11E+01	4.02E+01
	1MHZ	0.2024545	0.0795422	0.0673809	0.0557857	0.1122099
M'	1GHZ	0.2152537	0.2554927	0.2468301	0.3579872	0.2239255
	3GHZ	0.2240875	0.2500398	0.2493514	0.3561609	0.233999
	1MHZ	0.0331216	0.0572957	0.0546066	0.0579428	0.069395828
M''	1GHZ	0.0096803	0.007555	0.0066595	0.0175114	0.003252934
	3GHZ	0.0055598	0.012549	0.0038269	0.0035259	0.012147948

3.4.5.Real and Imaginary Electric Modulus

The electric modulus describes how grains and grain boundaries influence a materials dielectric properties. Within a specific frequency range, the real (M') and imaginary (M") parts of electric modulus are calculated by the following relation:

$$M' = \varepsilon' / \varepsilon'^2+\varepsilon''^2 \quad (16)$$
$$M'' = \varepsilon'' / \varepsilon'^2+\varepsilon''^2 \quad (17)$$

The M' and M" modulus of a prepared nanoferrites with the compositional formula $Ni_{0.3}Zn_{0.7}Pr_xFe_{2-x}O_4$(x=0.00, 0.025, 0.05, 0.075, and 0.1) was measured of the applied frequency 1MHz to 3GHz ranges. Electric modulus can be used to study the electrical reaction of ferroelectric materials, which is based on the phenomenon of electric complex modulus formalism can be used to describe grain and grain boundary effects in some homogeneous materials. The electric modulus of $Ni_{0.3}Zn_{0.7}PrxFe_{2-x}O_4$ is utilized to analyze the effects of interfacial polarization as a function of applied field frequency. The real part of electric modulus (M') is shown in the figure 7(a), and the imaginary part of electric modulus (M") is shown in figure 7(b).

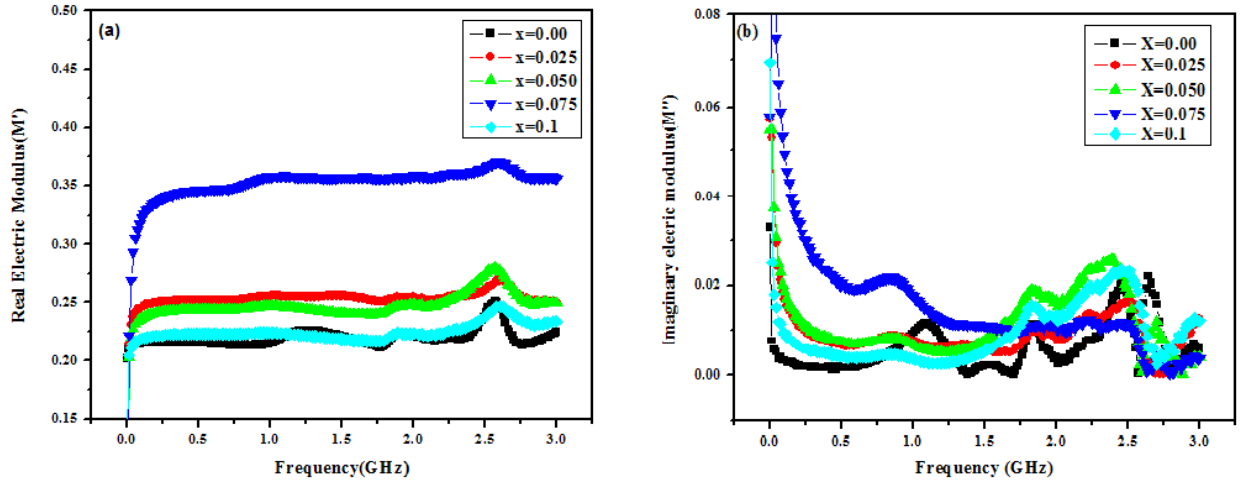

Figure 7: (a) The real electric modulus as function of frequency (b) The imaginary electric modulus as function of frequency

Figure 7(a) depicts the variance of the real part of modulus (M') with frequency. The value of M' increases with the increase in frequency, as seen in the graph. This is because the materials have a space charge polarization effect. The value of M' is increased then decreased at a certain frequency range of 1 MHz–3 GHz. Now from the figure 7(b) show that the Imaginary electric Modulus (M'') decreased with frequency increased. The

relationship between grain boundaries and peak formation confirms this perspective (Ditta, Khan, Junaid, Khalil, & Warsi, 2017).

4. Conclusions

Praseodymium (Pr^{3+}) doped Nickel−Zinc Ferrite having general formula $Ni_{0.3}Zn_{0.7}Pr_xFe_{2-x}O_4$ (x=0.00, 0.025, 0.050, 0.075 and 0.1) was synthesized via microemulsion technique, that is the easiest method to synthesizes of such type of ferrites. The FCC spinel structure is confirmed by XRD measurements. The XRD method was used to analyzed crystal structure and crystalline phase formation, and it's a great way to find out crystalline parameters including crystalline size, lattice parameters, x-ray density, and bulk density etc. The most intense peak of the XRD was identified at 2θ=35º. From Debye sherrer's formula, calculated the crystalline size 15nm to 29nm ranges. Lattice constant in the range of 8.360Å−8.380Å. The lattice parameter calculations are decreased with the doping of Praseodymium (Pr^{3+}) contents. Fourier Transform Infrared Spectroscopy (FTIR) technique was used to investigate spinel crystal structure of the prepared sample of composition $Ni_{0.3}Zn_{0.7}Pr_xFe_{2-x}O_4$ (x=0.00, 0.025, 0.050, 0.075 and 0.1). FTIR analyses reveal two frequency stretching bands υ_1 and υ_2 that correspond to the tetrahedral and octahedral sites respectively. The absorption bands υ_1 is known as octahedral stretching bands are found to be in the range of 414 cm^{-1} and υ_2 is the tetrahedral stretching band are found to be in the range of 530cm^{-1}. Dielectric properties of Praseodymium doped Nickel - Zinc Ferrite were measured with impedance analyzer from 1 MHz to 3 GHz frequency range. When Pr^{3+} concentration increases, the dielectric characteristics, such as dielectric constant (ε') and dielectric loss (ε'') and tangent loss was found to be decreases. The electric modulus describes how grains and grain boundaries influence a material's dielectric properties. Electric modulus can be used to study the electrical reaction of ferroelectric materials, which is based on the phenomenon of electric complex modulus formalism can be used to describe grain and grain boundary effects in some homogeneous materials. These measured dielectric characteristics showed that these nanomaterials may be used in higher frequencies devices.

Acknowledgement

We are grateful to ORIC of Balochistan University of Information Technology, Engineering and Management Sciences (BUITEMS), Quetta Pakistan.

References

Ahmed, M., Bishay, S. T., & Radwan, F. (2002). γ irradiation effect on the polarization and resistance of Li–Co–Yb-ferrite. *Journal of Physics and Chemistry of Solids, 63*(2), 279-286.

Al-Hilli, M. F., Li, S., & Kassim, K. S. (2009). Microstructure, electrical properties and Hall coefficient of europium-doped Li–Ni ferrites. *Materials Science and Engineering: B, 158*(1-3), 1-6.

Al-Hilli, M. F., Li, S., & Kassim, K. S. (2012). Structural analysis, magnetic and electrical properties of samarium substituted lithium–nickel mixed ferrites. *Journal of magnetism and magnetic materials, 324*(5), 873-879.

Aslam, S., Shifa, M. S., Gilani, Z. A., Usmani, M. N., Rehman, J. U., Khan, M. A., . . . Khalid, M. (2019). Structural, optical and magnetic elucidation of co-doping of Nd3+ and Pr3+ on lithium nanoferrite and its technological application. *Results in Physics, 12*, 1334-1339.

Batoo, K. M., Kumar, G., Yang, Y., Al-Douri, Y., Singh, M., Jotania, R. B., & Imran, A. (2017). Structural, morphological and electrical properties of Cd2+ doped MgFe2-xO4 ferrite nanoparticles. *Journal of Alloys and Compounds, 726*, 179-186.

Brightlin, B., & Balamurugan, S. (2016). The effect of post annealing treatment on the citrate sol–gel derived nanocrystalline BaFe 12 O 19 powder: Structural, morphological, optical and magnetic properties. *Applied Nanoscience, 6*(8), 1199-1210.

Ditta, A., Khan, M. A., Junaid, M., Khalil, R. A., & Warsi, M. F. (2017). Structural, magnetic and spectral properties of Gd and Dy co-doped dielectrically modified Co-Ni (Ni0. 4Co0. 6Fe2O4) ferrites. *Physica B: Condensed Matter, 507*, 27-34.

Gao, Y., Wang, Z., Pei, J., & Zhang, H. (2018). Structure and magnetic properties correlated with cation distribution of Ni0. 5-xMoxZn0. 5Fe2O4 ferrites prepared by sol-gel auto-combustion method. *Ceramics International, 44*(16), 20148-20153.

Gilani, Z. A., Warsi, M. F., Khan, M. A., Shakir, I., Shahid, M., & Anjum, M. N. (2015). Impacts of neodymium on structural, spectral and dielectric properties of LiNi0. 5Fe2O4 nanocrystalline ferrites fabricated via micro-emulsion technique. *Physica E: Low-dimensional Systems and Nanostructures, 73*, 169-174.

Iqbal, M. A., Islam, M., Ali, I., Sadiq, I., & Ali, I. (2014). High frequency dielectric properties of Eu+ 3-substituted Li–Mg ferrites synthesized by sol–gel auto-combustion method. *Journal of Alloys and Compounds, 586*, 404-410.

Jing, J., Liangchao, L., & Feng, X. (2007). Structural analysis and magnetic properties of Gd-doped Li-Ni ferrites prepared using rheological phase reaction method. *Journal of Rare Earths, 25*(1), 79-83.

Junaid, M., Khan, M. A., Iqbal, F., Murtaza, G., Akhtar, M. N., Ahmad, M., . . . Warsi, M. F. (2016). Structural, spectral, dielectric and magnetic properties of Tb–Dy doped Li-Ni nano-ferrites synthesized via micro-emulsion route. *Journal of magnetism and magnetic materials, 419*, 338-344.

Khan, M. A., Islam, M., Ishaque, M., & Rahman, I. (2011). Effect of Tb substitution on structural, magnetic and electrical properties of magnesium ferrites. *Ceramics International, 37*(7), 2519-2526.

Khan, M. A., Islam, M., Ishaque, M., & Rahman, I. (2012). Magnetic and dielectric behavior of terbium substituted Mg1− xTbxFe2O4 ferrites. *Journal of Alloys and Compounds, 519*, 156-160.

Lodhi, M. Y., Mahmood, K., Mahmood, A., Malik, H., Warsi, M. F., Shakir, I., . . . Khan, M. A. (2014). New Mg0. 5CoxZn0. 5− xFe2O4 nano-ferrites: structural elucidation and electromagnetic behavior evaluation. *Current Applied Physics, 14*(5), 716-720.

Parveen, A., Khalid, M., Gilani, Z. A., Aslam, S., Saleem, M., Shaikh, F. A., & Rehman, J. (2019). Dielectric, impedance and modulus spectroscopic studies of Co 0.3 Cd 0.7 Zn 1.5 x Fe 2− x O 4 nanoparticles. *Applied Physics A, 125*(10), 1-11.

Sheikh, F. A., Khalid, M., Shifa, M. S., Aslam, S., Perveen, A., ur Rehman, J., . . . Gilani, Z. A. (2019). Effects of bismuth on structural and dielectric properties of cobalt-cadmium spinel ferrites fabricated via micro-emulsion route. *Chinese Physics B, 28*(8), 088701.

Sun, C., & Sun, K. (2007). Preparation and microwave absorption properties of Ce-substituted lithium ferrite. *Solid state communications, 141*(5), 258-261.

Warsi, M. F., Gilani, Z. A., Al-Khalli, N. F., Sarfraz, M., Khan, M. A., Anjum, M. N., & Shakir, I. (2017). New LiNi0. 5PrxFe2− xO4 nanocrystallites: synthesis via low cost route for fabrication of smart advanced technological devices. *Ceramics International, 43*(17), 14807-14812.